A Nonintrusive Diagnostic Method for Open-Circuit Faults of Locomotive Inverters Based on Output Current Trajectory

Xun Wu, Rui Tian, Shu Cheng, Tefang Chen, and Li Tong

***Abstract*—Open-circuit (OC) fault diagnosis of voltage source inverters on trains still has two problems to be improved. First, it is usually forbidden to change the system structures of trains or to add any extra sensor. Therefore, diagnostic methods which need pulse width modulation control signals or extra output voltage sensors are no longer suitable for trains. Second, loads on the train vary in a wide range and have significant influence on output currents. In order to solve these problems and increase the maintenance efficiency, an online diagnostic method for single switch OC (SSOC) faults and double switches OC (DSOC) faults is proposed. Supposing that three phases are balanced, it is proved that the trajectory of two output currents is an ellipse in the Cartesian coordination, and each OC fault has a unique trajectory. SSOC faults and DSOC faults can be isolated by detecting abnormal slopes and directions of several consecutive points on the trajectory. The fastest diagnostic process takes less than half a period. Load variation has impact on the size and shape of the trajectory but does not affect the diagnostic method. Experimental tests are carried out on dSPACE platform. Results show the accuracy of the mathematical model and the effectiveness of the online diagnostic method proposed in this paper.**

***Index Terms*—Fault currents, fault diagnosis, fault location, inverters.**

I. Introduction

THREE-PHASE inverters convert dc inputs into ac outputs. They are not only widely used as the uninterrupted power supplies in many situations such as military, communications, and factories, but also play a significant role in energy conversion of high-speed trains. Due to the high-frequency switching of power switches, inverters are very sensitive and susceptible when they are working. For instance, inverter failures account for a large part of motor variable frequency speed regulation system faults [1]. They are mainly caused by the failure of power switches in most cases [2]. Short-circuit faults of power switches can be converted to open-circuit (OC) faults by serial fast fuses [3]. Therefore, power switch failures are usually shown in the form of OC faults. A real-time method for condition monitoring and fault diagnosis is needed to detect and isolate OC faults quickly when they occur.

Several papers have been published proposing diagnostic methods in single-phase inverters. Kamel *et al*. [4] divided OC faults into insulated gate bipolar transistors (IGBTs) failures and gate driver faults, and diagnosed these faults by phase currents. They also proposed a method based on adaptive neural-fuzzy inference system to detect and isolate OC faults [5]. Moreover, Kamel *et al*. [6] proposed a sensor-less diagnostic technique based on spectrum analysis. Xiao and Li [7] presented a diagnostic method based on spectral decomposition. Faults are detected through the identification of voltages and currents.

Researchers mainly focus on the three-phase inverters. The diagnostic strategies based on currents detection were found in a number of papers. Zidani *et al*. [8] introduced a fault detection and diagnosis based on fuzzy logic for pulse width modulation (PWM) voltage source inverters. This diagnosis requires the measurement of output currents to detect intermittent loss of firing pulses in the inverter power switches. Sleszynski *et al*. [9] suggested combining the normalized dc components with additional diagnostic variables, the percentage of time spent by the phase currents in the near-zero zone, to diagnose OC faults. The certainty of the diagnoses under transients and light loads has been markedly improved. Estima and Cardoso [10] presented a diagnostic technique based on the errors of the normalized currents average absolute values, providing a very high immunity against false alarms. Espinoza-Trejo *et al*. [11] proposed a PI observer-based fault detection and isolation (FDI) scheme to diagnose actuator faults in voltage-source inverter (VSI) for induction motor (IM). Nonlinear PI observers were used to identify the dc component of the fault profiles. This method needs information of stator currents and mechanical position. Jung *et al*. [12] introduced a simple and low-cost OC fault identification method for PWM voltage source inverters employing a permanent magnet synchronous motor. The method employs the model reference adaptive system techniques and requires two current sensors and a position sensor. Faults were detected by voltage

Manuscript received October 31, 2016; revised February 18, 2017 and April 11, 2017; accepted May 22, 2017. Date of publication June 2, 2017; date of current version February 1, 2018. This work was supported in part by the National Natural Science Foundation of China under Grant 61273158, in part by the National Key R & D Plan under Grant 2016YFB1200401, and in part by the Fundamental Research Funds for the Central Universities of Central South University under Grant 2017zzts202. Recommended for publication by Associate Editor Julia Zhang. *(Corresponding author: Shu Cheng.)*

X. Wu and R. Tian are with the School of Information Science and Engineering, Central South University, Changsha 410075, China (e-mail: 309931624@qq.com; 315684379@qq.com).

S. Cheng and T. Chen are with the School of Traffic and Transportation Engineering, Central South University, Changsha 410075, China (e-mail: 6409020@qq.com; ctfcyt@163.com).

L. Tong is with the China Academy of Railway Sciences Locomotive Car Research Institute, Beijing 100081, China (e-mail: carstongli@qq.com).

Color versions of one or more of the figures in this paper are available online at http://ieeexplore.ieee.org.

Digital Object Identifier 10.1109/TPEL.2017.2711598

distortion observer. An *et al*. [13] presented a diagnostic method based on current residual vector for closed-loop controlled permanent magnet synchronous motor (PMSM) drive systems. The technique can get rid of effects of the load and the main controller. Similarly, two current sensors and a position sensor are needed. Wu *et al*. [14] introduced a symmetry-analysis-based diagnosis method. Correlation coefficients of two phase currents are used to describe the symmetry of the inverter under healthy and fault conditions, and mean values of current samples during a period are used to isolate fault switches. Eickhoff *et al*. [15] suggested diagnosing OC faults by the observation of the current control deviation and a subsequent test procedure. Huang *et al*. [16] proposed an OC fault diagnostic method based on the instant current vector rotating angles. The method is fair robust to load changes and variable speed. Hu *et al.* [17] proposed a wavelet entropy-based OC fault diagnosis for traction inverters. The method shows that five entropy forms are superior to traditional fault detections and fault can be isolated by the best entropy form. Gou *et al*. [18] presented a load current based approach and fault tolerance technique for high-speed railway electrical traction drive system.

There are many OC fault diagnostic methods based on voltage detection or other signals as well. Lúcio de Araujo Ribeiro *et al*. [19] suggested detecting OC faults through a direct comparison of the measured voltages to their reference voltages obtained from the PWM reference signals. They also introduced four detection techniques in the paper. Karimi *et al*. [20] proposed a technique based on field–programmable gate array (FPGA). Power switch failures are detected in less than 10 μs by the comparison between measured and estimated pole voltages. An *et al*. [21] proposed a diagnostic method based on the switching function model of the inverter under both healthy and faulty conditions. OC faults can be detected by the collector–emitter voltage of lower power switch in each leg. Hang *et al*. [22] suggested utilizing zero-order voltage to detect open-phase faults for permanent magnet synchronous motor drive system. The threshold and counting are used to enhance the robustness of the method. Abul Masrur *et al*. [23] proposed a machine learning technique for fault diagnosis. A neural network was used to isolate single switch OC (SSOC) faults, post-short-circuits, short circuits, and the unknown faults. Li *et al*. [24] presented an OC fault diagnosis based on several state observers and a new fault-tolerant approach to reduce output distortion. Salehifar and Moreno-equilaz [25] introduced a novel diagnostic method and a fault-tolerant technique for voltage source inverters.

There are different kinds of IGBT modules in the market such as single switch, dual, and six-packed. When the IGBT module is double- or six-packed, the failure of one IGBT may lead to faults of others. These kinds of faults have occurred on traction inverters several times. Some researchers have studied fault diagnostic techniques for multiple OC faults and shared their achievements. In [9] and [16], researchers detected multiple OC faults through analyzing the trajectories obtained by three stator current vectors. Estima and Cardoso [10] achieved the detection by the errors of the normalized currents average absolute values. Wu and Zhao [26] introduced a diagnostic technique based on allelic points and its criterion to isolate multiple OC faults. Zhang

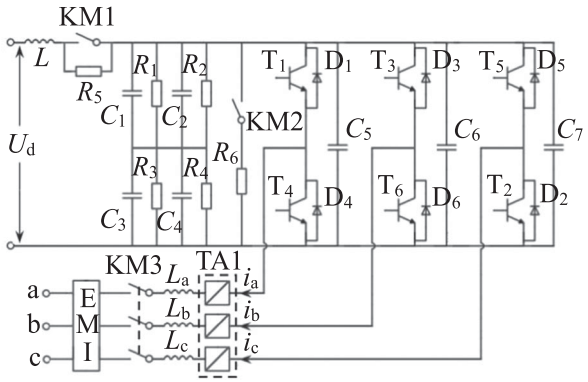

Fig. 1. Inverter structure of type 25T train.

et al. [27] presented a single and double switches OC (DSOC) fault detection method based on d- and q-axis current repetitive distortions. The distortions are estimated and compared with the threshold value to detect the fault, and two current sensors and a speed sensor are required. Trabelsi *et al.* [28] suggested detecting multiple OC faults by analyzing the PWM switching signals and the line-to-line voltage levels during the switching times.

Although these studies on OC faults have their own advantages, there are still some problems remaining to be solved for locomotive inverters. First, intrusive modifications are usually forbidden for the sake of security of the train. In other words, it is not allowed to acquire control signals or install additional sensors. Second, loads of the locomotive inverter have a wide range of variation. Diagnostic methods that are susceptible to load variation are no longer suitable for these inverters. Therefore, the fault diagnosis of locomotive inverters needs further study. In this paper, an online diagnostic method suitable for locomotive inverters is proposed to solve the above-mentioned problems. It can accurately locate fault switches in a short time, effectively make up for the shortage of regular maintenance, and greatly reduce the overhaul cost.

In the paper, a precise mathematical model is derived from two output currents obtained by the existing current sensors installed in the inverter on a Type 25T train. Assuming that three phases are balanced, it is proved that the trajectory of two output currents is an ellipse in the Cartesian coordination, and each OC fault has a unique trajectory. SSOC faults and DSOC faults can be isolated by detecting abnormal slopes and directions of several consecutive points on the trajectory. Load variation has impact on the size and shape of the trajectory but does not affect the diagnostic method. The whole diagnosis process can be completed without control signals. Experimental tests are carried out on dSPACE platform. It is shown that the model is accurate and the method is effective and robust to load variation.

II. System Overview

A. Operational Principle of the System

The inverter structure of Type 25T train is shown in Fig. 1. The input voltage is dc 600 V. The output voltages are

three-phase ac 380 V, with the frequency of 50 Hz. Sinusoidal pulse width modulation (SPWM) is adopted and switching frequency is 3 kHz. The charge buffer circuit consists of L, R_5, and KM1. DC-side capacitor support is composed of $C_1 - C_4$ and $R_1 - R_4$. The discharge circuit includes R_6 and KM2. When dc-side voltage U_d is lower than dc 500 V, KM1 and KM3 will be turned OFF, and KM2 will be turned ON. KM1 will be turned ON and KM2 will be turned OFF once U_d is over dc 500 V. KM3 will be turned ON and the inverter will start to work after the precharging is accomplished. $T_1 - T_6$ are IGBTs and $D_1 - D_6$ are additional reverse parallel diodes for IGBTs. $C_5 - C_7$ are noninductive capacitors. Three-phase currents i_a, i_b, and i_c are measured by current sensors TA1. Electromagnetic interference is used for filtering.

B. General Idea of the Diagnostic Method

This paper focuses on the isolation of SSOC faults and DSOC faults. It is easy to know that an ellipse will be presented when two trigonometric functions with the same frequency and a phase difference are combined in a Cartesian coordinate. This ellipse combines most of the information contained by the two trigonometric functions. Thus, OC faults can be located accurately by the distortion of the ellipse generated by two output currents or voltages. There are two line voltage sensors installed on the train to monitor voltages u_{ab} and u_{bc}. If these voltages are used for diagnosis, it is difficult to obtain functions of fault voltage waves. They will bring much difficulty to theoretical analysis and modeling. Besides, fault features of some trajectories are easily confused (such as T_1 OC fault and T_5 OC fault) and will have certain impact on fault isolation. Although load variation has influence on output currents, the functions are simple and clear, the theoretical analysis and modeling are much easier. When an OC fault occurs, the output current of the corresponding phase is approximately close to zero in nearly half-period. For example, if T_1 OC fault occurs, the current i_a in Fig. 1 will be close to zero in the half-current cycle due to the failure of the upper arm, and i_a will be normal when it is negative. On the contrary, if T_4 OC fault occurs, the current i_a will be approximately equal to zero in the half-current cycle due to the failure of the lower arm, and i_a will be normal when it is positive. Moreover, the influence of load variation can be eliminated by analyzing the features of the distortion. Therefore, two output currents rather than two output voltages are utilized as the fault signals in this paper.

III. A–B Trajectory and Its Properties

In Fig. 1, three-phase currents are sine waves with equal magnitudes and a difference of 120°

$$\begin{cases} i_a = I_{am}\sin(\omega t) \\ i_b = I_{bm}\sin(\omega t + \phi) \\ i_c = I_{cm}\sin(\omega t + 2\phi) \end{cases} \tag{1}$$

where I_{am}, I_{bm}, and I_{cm} are magnitudes of i_a, i_b, and i_c, respectively. ω is fundamental frequency. $\omega t > 0$. ϕ is the phase difference.

Define $x = i_a(t)$, $y = i_b(t)$, then

$$\begin{cases} x = I_{am}\sin(\omega t) = I_{am}\cos\left(\frac{\pi}{2} - \omega t\right) \\ y = I_{bm}\sin(\omega t + \phi) \end{cases}. \tag{2}$$

Here, $x \in [-I_{am}, I_{am}]$, $y \in [-I_{bm}, I_{bm}]$. The product of ω and t is obtained from (2)

$$\begin{cases} \omega t = \frac{\pi}{2} - \cos^{-1}\left(\frac{x}{I_{am}}\right) \\ \omega t = \sin^{-1}\left(\frac{y}{I_{bm}}\right) - \phi \end{cases}. \tag{3}$$

Cancel ωt and combine the two equations, the relationship between x and y can be given by (3)

$$\phi + \frac{\pi}{2} = \cos^{-1}\left(\frac{x}{I_{am}}\right) + \sin^{-1}\left(\frac{y}{I_{bm}}\right). \tag{4}$$

Sin of (4) is

$$\cos\phi = \sin\left[\cos^{-1}\left(\frac{x}{I_{am}}\right)\right]\cdot\cos\left[\sin^{-1}\left(\frac{y}{I_{bm}}\right)\right] + \frac{x}{I_{am}}\cdot\frac{y}{I_{bm}}. \tag{5}$$

For the right part of (5), we have

$$\sin\left[\cos^{-1}\left(\frac{x}{I_{am}}\right)\right] = \sqrt{1-\cos^2\left[\cos^{-1}\left(\frac{x}{I_{am}}\right)\right]} = \sqrt{1-\left(\frac{x}{I_{am}}\right)^2}. \tag{6}$$

$$\cos\left[\sin^{-1}\left(\frac{y}{I_{bm}}\right)\right] = \sqrt{1-\sin^2\left[\sin^{-1}\left(\frac{y}{I_{bm}}\right)\right]} = \sqrt{1-\left(\frac{y}{I_{bm}}\right)^2}. \tag{7}$$

Thus, (5) can be expressed as

$$\cos(\phi) - \frac{x}{I_{am}}\cdot\frac{y}{I_{bm}} = \sqrt{\left[1-\left(\frac{x}{I_{am}}\right)^2\right]\left[1-\left(\frac{y}{I_{bm}}\right)^2\right]}. \tag{8}$$

Both sides of (8) are squared; then, an ellipse is established

$$\frac{x^2}{I_{am}^2} + \frac{y^2}{I_{bm}^2} - \frac{2\cos(\phi)}{I_{am}\cdot I_{bm}}\cdot xy - \sin^2(\phi) = 0$$
$$x \in [-I_{am},\ I_{am}],\ y \in [-I_{bm},\ I_{bm}]. \tag{9}$$

According to the general equation of ellipse, it follows:

$$A = \frac{1}{I_{am}^2},\ B = -\frac{2\cos(\phi)}{I_{am}\cdot I_{bm}},\ C = \frac{1}{I_{bm}^2},$$
$$D = E = 0,\ F = -\sin^2(\phi). \tag{10}$$

Because

$$B^2 - 4AC = \frac{4\cos^2(\phi)}{I_{am}^2\cdot I_{bm}^2} - \frac{4}{I_{am}^2\cdot I_{bm}^2} < 0. \tag{11}$$

Thus, (9) agrees with the general equation of ellipse in the Cartesian coordination. The center is located at the origin of

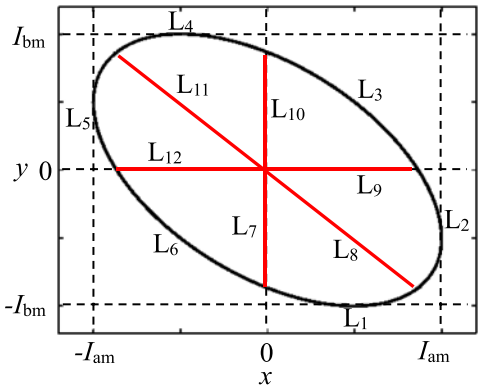

Fig. 2. *A–B* trajectories under all conditions.

coordinate. The pattern drawn by (9) is called *a–b* trajectory under normal operations.

Suppose $I_{am} = I_{bm}$, the angle and centrifugal rate of *a–b* trajectory can be obtained as follows:

$$\theta = \frac{1}{2}\arcsin\left(-\frac{B}{\sqrt{(A-C)^2+B^2}}\right) = -\frac{\pi}{4} \tag{12}$$

$$e^2 = \frac{2\sqrt{(A-C)^2+B^2}}{A+C+\sqrt{(A-C)^2+B^2}} = \frac{2}{1+\left|\frac{1}{\cos(\phi)}\right|}. \tag{13}$$

The distance from any point on the ellipse to the origin is

$$d = \sqrt{x^2+y^2} = I_{am}\sqrt{\sin^2(\omega t)+\sin^2(\omega t+\phi)}. \tag{14}$$

It can be drawn that, under ideal situation, *a–b* trajectory is an oblique ellipse with an angle of $-\pi/4$. The centrifugal rate is related to ϕ. When ω and ϕ are fixed, d is proportional to the magnitudes of load currents.

IV. Fault Analysis

The *a–b* trajectories under all conditions are shown in Fig. 2. $L_1 - L_{12}$ are 12 parts of the trajectories. The black lines and red lines are normal parts and fault parts of the trajectory, respectively. *A–B* trajectories of SSOC faults and DSOC faults are analyzed in the following sections.

A. Single Switch Open-Circuit Faults

When T_1 OC fault occurs, i_a and i_b are

$$i_a(t) = \begin{cases} 0 & \omega t \in [2k\pi, 2k\pi+\pi) \\ I_{am}\sin(\omega t) & \omega t \in [2k\pi+\pi, 2k\pi+2\pi) \end{cases} \tag{15}$$

$$i_b(t) = I_{bm}\sin(\omega t+\phi) \quad \omega t \in [2k\pi, 2k\pi+2\pi) \tag{16}$$

where k is a natural number. Under this condition, $x \in [-I_{am}, 0]$, $y \in [-I_{bm}, I_{bm}]$. The ellipse has distorted. The *a–b* trajectory can be obtained from (9): eq. (17) as shown at the bottom of the page.

The *a–b* trajectory can be expressed as FAULT_T1 $= [L_4\ L_5\ L_6\ L_7\ L_{10}]$ in Fig. 2.

When T_4 OC fault occurs, i_a and i_b are

$$i_a(t) = \begin{cases} I_{am}\sin(\omega t) & \omega t \in [2k\pi, 2k\pi+\pi) \\ 0 & \omega t \in [2k\pi+\pi, 2k\pi+2\pi) \end{cases} \tag{18}$$

$$i_b(t) = I_{bm}\sin(\omega t+\phi) \quad \omega t \in [2k\pi, 2k\pi+2\pi). \tag{19}$$

In this case, $x \in [0, I_{am}]$, $y \in [-I_{bm}, I_{bm}]$. The distorted ellipse is (20) as shown at the bottom of the page.

The *a–b* trajectory can be expressed as FAULT_T4 $= [L_1\ L_2\ L_3\ L_{10}\ L_7]$ in Fig. 2.

In the same way, when $T3$ or T_6 OC fault occurs, the *a–b* trajectory can be expressed as FAULT_T3 $= [L_6\ L_1\ L_2\ L_9\ L_{12}]$ or FAULT_T6 $= [L_3\ L_4\ L_5\ L_{12}\ L_9]$ in Fig. 2.

When T_5 OC fault occurs, i_c is (21) as shown at the bottom of the page.

According to the relationship of three-phase currents

$$i_a + i_b + i_c = 0. \tag{22}$$

If $i_c = 0$, then

$$i_a + i_b = 0. \tag{23}$$

Thus, the distorted ellipse is (24) as shown at the bottom of the next page.

The *a–b* trajectory can be expressed as FAULT_T5 $= [L_2\ L_3\ L_4\ L_{11}\ L_8]$ in Fig. 2.

When T_2 OC fault occurs, i_c is (25) as shown at the bottom of the next page.

The distorted ellipse is (26) as shown at the bottom of the next page.

The *a–b* trajectory can be expressed as FAULT_T2 $= [L_5\ L_6\ L_1\ L_8\ L_{11}]$ as shown in Fig. 2.

$$\begin{cases} \frac{y^2}{I_{bm}^2} - \sin^2(\phi) = 0 & \omega t \in [2k\pi, 2k\pi+\pi) \\ \frac{x^2}{I_{am}^2} + \frac{y^2}{I_{bm}^2} - \frac{2\cos(\phi)}{I_{am}\cdot I_{bm}}\cdot xy - \sin^2(\phi) = 0 & \omega t \in [2k\pi+\pi, 2k\pi+2\pi) \end{cases} \tag{17}$$

$$\begin{cases} \frac{x^2}{I_{am}^2} + \frac{y^2}{I_{bm}^2} - \frac{2\cos(\phi)}{I_{am}\cdot I_{bm}}\cdot xy - \sin^2(\phi) = 0 & \omega t \in [2k\pi, 2k\pi+\pi) \\ \frac{y^2}{I_{bm}^2} - \sin^2(\phi) = 0 & \omega t \in [2k\pi+\pi, 2k\pi+2\pi) \end{cases} \tag{20}$$

$$i_c(t) = \begin{cases} 0 & \omega t \in [2k\pi-2\phi, 2k\pi-2\phi+\pi) \\ I_{cm}\sin(\omega t+2\phi) & \omega t \in [2k\pi-2\phi+\pi, 2k\pi-2\phi+2\pi) \end{cases} \tag{21}$$

TABLE I
A–B TRAJECTORIES OF SSOC FAULTS

Faulty number	SSOC fault	*a–b* trajectory
1	T_1	FAULT_T1 = $[L_4\ L_5\ L_6\ L_7\ L_{10}]$
2	T_2	FAULT_T2 = $[L_5\ L_6\ L_1\ L_8\ L_{11}]$
3	T_3	FAULT_T3 = $[L_6\ L_1\ L_2\ L_9\ L_{12}]$
4	T_4	FAULT_T4 = $[L_1\ L_2\ L_3\ L_{10}\ L_7]$
5	T_5	FAULT_T5 = $[L_2\ L_3\ L_4\ L_{11}\ L_8]$
6	T_6	FAULT_T6 = $[L_3\ L_4\ L_5\ L_{12}\ L_9]$

Table I lists all the *a–b* trajectories of SSOC faults. The *a–b* trajectory of each OC fault is unique. It can be found that if SSOC faults of two switches in a phase occur simultaneously, *a–b* trajectories of them are complementary because of the complementary conduction time.

B. Double Switches Open-Circuit Faults

Six switches are independent in topological structure of an inverter. The correlation coefficient of any two switches is zero. Therefore, the effect of SSOC faults is independent. From the mathematical theory, the effect of DSOC fault can be obtained by the superposition of effect caused by the corresponding two SSOC faults.

For instance

$$\text{If } \mathrm{T}_1 \text{ OC fault occurs, then } x \in [-I_{am}, 0], y \in [-I_{bm}, I_{bm}];$$

$$\text{If } T_4 \text{ OC fault occurs, then } x \in [0, I_{am}], y \in [-I_{bm}, I_{bm}].$$

When T_1 and T_4 OC faults occur, x and y must agree with all constrains mentioned above at the same time. Then

$$x = 0,\ y \in [-I_{bm}, I_{bm}].$$

The *a–b* trajectory derived from (15–20) is a closed curve on the Y axis. All the *a–b* trajectories of DSOC faults can be obtained by the following formula:

$$\text{FAULT\_T}i\&\text{T}j = \text{FAULT\_T}i \cap \text{FAULT\_T}j \tag{27}$$

where Ti and Tj are two different switches of an inverter. The symbol "$\cap$" means that FAULT_Ti&Tj is the boundary line of the overlapping part of the two regions enclosed by FAULT_Ti and FAULT_Tj. For example, DSOC fault of T_1 and T_4 can be calculated by (27):

$$\begin{aligned}\text{FAULT\_T1\&}T4 &= \text{FAULT\_T1} \cap \text{FAULT\_T4} \\ &= [L_7 L_{10} L_{10} L_7].\end{aligned}$$

TABLE II
A–B TRAJECTORIES OF DSOC FAULTS

Faulty number	DSOC fault	*a–b* trajectory
7	T_1 and T_2	FAULT_T1&T2 = $[L_5\ L_6\ L_7\ L_{11}]$
8	T_1 and T_3	FAULT_T1&T3 = $[L_6\ L_7\ L_{12}]$
9	T_1 and T_4	FAULT_T1&T4 = $[L_7\ L_{10}\ L_{10}\ L_7]$
10	T_1 and T_5	FAULT_T1&T5 = $[L_4\ L_{11}\ L_{10}]$
11	T_1 and T_6	FAULT_T1&T6 = $[L_4\ L_5\ L_{12}\ L_{10}]$
12	T_2 and T_3	FAULT_T2&T3 = $[L_6\ L_1\ L_8\ L_{12}]$
13	T_2 and T_4	FAULT_T2&T4 = $[L_1\ L_8\ L_7]$
14	T_2 and T_5	FAULT_T2&T5 = $[L_{11}\ L_8\ L_8\ L_{11}]$
15	T_2 and T_6	FAULT_T2&T6 = $[L_5\ L_{12}\ L_{11}]$
16	T_3 and T_4	FAULT_T3&T4 = $[L_1\ L_2\ L_9\ L_7]$
17	T_3 and T_5	FAULT_T3&T5 = $[L_2\ L_9\ L_8]$
18	T_3 and T_6	FAULT_T3&T6 = $[L_{12}\ L_9\ L_9\ L_{12}]$
19	T_4 and T_5	FAULT_T4&T5 = $[L_2\ L_3\ L_{10}\ L_8]$
20	T_4 and T_6	FAULT_T4&T6 = $[L_3\ L_{10}\ L_9]$
21	T_5 and T_6	FAULT_T5&T6 = $[L_3\ L_4\ L_{11}\ L_9]$

Table II lists all the *a–b* trajectories obtained by (27). The *a–b* trajectory of each DSOC fault is different from others. Moreover, some *a–b* trajectories of DSOC faults show a symmetry. For one kind of DSOC fault, two switches in different phases fail. For the other kind of DSOC fault, the complementary two switches in these two phases fail. Then, *a–b* trajectories of these two kinds of DSOC faults are origin-symmetric.

From Tables I and II, it is concluded that there are 21 kinds of *a–b* trajectories corresponding to 21 kinds of OC faults. For each fault, it can be isolated accurately by identifying the *a–b* trajectory.

For three switches OC faults, *a–b* trajectories can be deduced in the same way, and are different from those of SSOC faults or DSOC faults. However, it is difficult to isolate all the three switches OC faults by just two currents. It is also senseless to isolate three faulty switches because the inverter has nearly broken down. Fault analysis of three switches OC faults is not discussed in this paper.

V. FAULT DIAGNOSTIC METHOD

The trajectory is composed of points which move counterclockwise. It can be seen from Fig. 2 that the trajectory will pass through some of the red lines (L_7, L_8, L_9, L_{10}, L_{11}, L_{12}) and the origin when OC fault occurs. The trajectory can pass through these red lines in six different directions, which include the X-axis direction ($\rightarrow$), the negative direction of X axis ($\leftarrow$), the Y-axis direction ($\uparrow$), the negative direction of Y axis ($\downarrow$), the increasing direction of X axis along the line $x + y = 0$ ($\searrow$),

$$\begin{cases} x + y = 0 & \omega t \in [2k\pi - 2\phi, 2k\pi - 2\phi + \pi) \\ \frac{x^2}{I_{am}^2} + \frac{y^2}{I_{bm}^2} - \frac{2\cos(\phi)}{I_{am} \cdot I_{bm}} \cdot xy - \sin^2(\phi) = 0 & \omega t \in [2k\pi - 2\phi + \pi, 2k\pi - 2\phi + 2\pi) \end{cases} \tag{24}$$

$$i_c(t) = \begin{cases} I_{cm} \sin(\omega t + 2\phi) & \omega t \in [2k\pi - 2\phi, 2k\pi - 2\phi + \pi) \\ 0 & \omega t \in [2k\pi - 2\phi + \pi, 2k\pi - 2\phi + 2\pi) \end{cases} \tag{25}$$

$$\begin{cases} \frac{x^2}{I_{am}^2} + \frac{y^2}{I_{bm}^2} - \frac{2\cos(\phi)}{I_{am} \cdot I_{bm}} \cdot xy - \sin^2(\phi) = 0 & \omega t \in [2k\pi - 2\phi, 2k\pi - 2\phi + \pi) \\ x + y = 0 & \omega t \in [2k\pi - 2\phi + \pi, 2k\pi - 2\phi + 2\pi) \end{cases} \tag{26}$$

TABLE III
DIRECTIONS OF SSOC FAULTS AND DSOC FAULTS

Fault switch	Direction	Fault switch	Direction	Fault switch	Direction
T_1	↑	T_1 and T_3	↑←	T_2 and T_6	↖→
T_2	↖	T_1 and T_4	↑↓	T_3 and T_4	←↓
T_3	←	T_1 and T_5	↑↘	T_3 and T_5	←↘
T_4	↓	T_1 and T_6	↑→	T_3 and T_6	←→
T_5	↘	T_2 and T_3	↖←	T_4 and T_5	↓↘
T_6	→	T_2 and T_4	↖↓	T_4 and T_6	↓→
T_1 and T_2	↑↖	T_2 and T_5	↖↘	T_5 and T_6	↘→

TABLE IV
DIRECTION JUDGMENT DURING OC FAULTS

Abnormal slope	Vector $(\Delta x, \Delta y)$	Direction
$k_x = 1$	$\Delta x > 0$	→
	$\Delta x < 0$	←
$k_y = 1$	$\Delta y > 0$	↑
	$\Delta y < 0$	↓
$k_{xy} = 1$	$\Delta x > 0$ or $\Delta y < 0$	↘
	$\Delta x < 0$ or $\Delta y > 0$	↖

and the decreasing direction of X axis along the line $x + y = 0$ (↖).

For SSOC faults, there is only one direction when the trajectory passes the red lines. For DSOC faults, there are two different directions when the trajectory passes the red lines. Table III presents directions of these faults. Therefore, SSOC faults and DSOC faults can be isolated by directions of these red lines.

A. Fault Detection

There are two abnormalities of the trajectory when OC fault occurs: origin crossing and slope anomaly.

Origin crossing: under normal operating conditions, the trajectory is an ellipse that surrounds but does not pass through the origin, we define *origin_corssing* $= 0$. When OC fault occurs and the trajectory passes the origin, we define *origin_corssing* $= 1$.

Slope anomaly: slope k of the point on the trajectory to the origin is close to 0, ∞, or –1. The definitions of these three abnormal slopes are:

1) if $|k| < \tan(\alpha)$, then $k_x = 1$, else $k_x = 0$;
2) if $|k| > \tan(\pi/2 - \alpha)$, then $k_y = 1$, else $k_y = 0$;
3) if $-\tan(\pi/4 + \alpha) < k < -\tan(\pi/4 - \alpha)$, then $k_{xy} = 1$, else $k_{xy} = 0$;

where $0 < \alpha < \pi/8$. Note that a slope anomaly is detected only when slopes of several consecutive points on the trajectory to the origin satisfy one of the three conditions mentioned above, otherwise, normal points may be regarded as fault points in some cases.

Therefore, fault signal can be expressed as

$$Fault = (origin\_crossing \text{ OR } k_x \text{ OR } k_y \text{ OR } k_{xy}) \quad (28)$$

where OR is the logic operation. When OC fault is detected, then *Fault* $= 1$, otherwise, *Fault* $= 0$.

B. Fault Isolation

Actually, OC faults are isolated by fault time, abnormal slopes, and directions of the trajectory. Each direction can be determined by an abnormal slope and a point on the current trajectory. In this paper, three points A (x_A, y_A), B (x_B, y_B), and C (x_C, y_C) are utilized to calculate the two directions. Point A is the fault point before the trajectory passes through the origin. Point B is the origin (0, 0). Point C is the fault point after the trajectory passes through the origin. Then, vectors $\overrightarrow{AB}$ and $\overrightarrow{BC}$ can be expressed as

$$\begin{cases} \overrightarrow{AB} = (x_B - x_A,\ y_B - y_A) = (-x_A,\ -y_A) \\ \overrightarrow{BC} = (x_C - x_B,\ y_C - y_B) = (x_C,\ y_C) \end{cases}. \quad (29)$$

Define Δx as $x_B - x_A$ or $x_C - x_B$, Δy as $y_B - y_A$ or $y_C - y_B$. Table IV lists the direction judgment during OC faults.

For SSOC faults, the fault time of each cycle is no more than half of the period T_s. There is only one direction and one abnormal slope. Then, we have

$$\begin{cases} k_x + k_y + k_{xy} = 1 \\ t_{Fault} \le T_s/2 \end{cases}. \quad (30)$$

The direction can be determined as long as point A or C is obtained. Generally, it is not suitable to determine the direction by the point obtained at the time when the OC fault just occurs (the rising edge of *Fault*), because the fault occurrence time is unknown and this point may not be A. Otherwise, the other switch of the same phase may be regarded as the fault switch incorrectly. However, the point obtained at the falling edge of *Fault* must be point C. Thus, vector $\overrightarrow{BC}$ and the direction can be determined. The fault switch can be isolated by the direction according to Table III.

For DSOC faults in the same phase, the fault time of each cycle is over half of the period T_s. There are two directions but only one abnormal slope. Then, we have

$$\begin{cases} k_x + k_y + k_{xy} = 1 \\ t_{Fault} > T_s/2 \end{cases}. \quad (31)$$

These DSOC faults can be isolated by the duration of the abnormal slope:

if $t_{Fault} > T_s/2$ and $k_x = 1$, then phase b fails, fault switches are T_3 and T_6;

if $t_{Fault} > T_s/2$ and $k_y = 1$, then phase a fails, fault switches are T_1 and T_4;

if $t_{Fault} > T_s/2$ and $k_{xy} = 1$, then phase c fails, fault switches are T_2 and T_5.

For DSOC faults in different phases, there are two different directions and two different abnormal slopes. Then, we have

$$k_x + k_y + k_{xy} = 2. \quad (32)$$

Both point A and point C are needed to calculate the two directions. A point is sampled when a new abnormal slope is detected. When DSOC faults in different phases occur, the first abnormal slope k_1 is detected, then $k_1 = 1$, otherwise $k_1 = 0$;

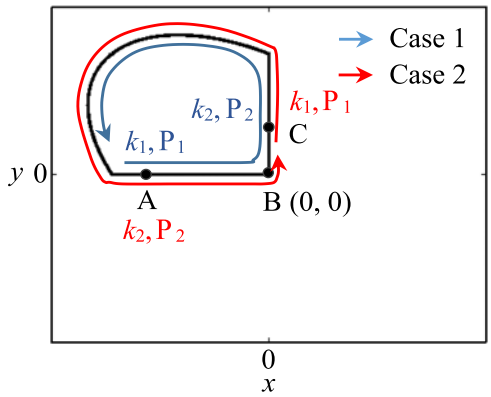

Fig. 3. Influence of the fault occurrence time on the positions of P_1 and P_2.

a new abnormal slope k_2 will be detected after some time, then $k_2 = 1$, otherwise $k_2 = 0$. Two points P_1 and P_2 used for direction calculation are sampled at the rising edges of k_1 and k_2, respectively. Similarly, the uncertainty of fault occurrence time makes it difficult to determine which of the two points is A or C. If faults occur before the trajectory passes point B (case 1 in Fig. 3), then P_1 is A and P_2 is C. If faults occur after the trajectory passes point B (case 2 in Fig. 3), then P_1 is C and P_2 is A. Therefore, it is necessary to determine the relationship among P_1, P_2, A, and C before direction calculations.

Since point B is between A and C, P_1 and P_2 can be identified by the order of the three points and the location of point B. Define t_1 as the time from the rising edge of *Fault* to the rising edge of k_1, t_2 the time from the rising edge of *Fault* to the rising edge of k_2, t_B the time from the rising edge of *Fault* to the rising edge of *origin_crossing*, then we have:

if $t_1 < t_B < t_2$, then P_1 is A and P_2 is C;
if $t_B < t_1 < t_2$, then P_1 is C and P_2 is A;
if $t_1 < t_2 < t_B$, then P_1 is C and P_2 is A.
Therefore:
if $(t_B - t_1)(t_B - t_2) < 0$, then P_1 is A and P_2 is C;
if $(t_B - t_1)(t_B - t_2) > 0$, then P_1 is C and P_2 is A.

When points A and C are obtained, two different directions can be determined, then fault switches can be isolated by the two directions according to Table III.

The diagnosis process is introduced in Fig. 4. During the process, directions are calculated at first, then the fault isolation module decides which data to use for diagnosis according to the values of k_x, k_y, k_{xy}, and t_{Fault}. For SSOC faults, the origin-crossing and abnormal slopes are detected by x and y when fault occurs. Then, *origin-crossing* and the corresponding abnormal slopes are set to 1. *Fault* is obtained through logic operation. Next, point C is detected at the falling edge of *Fault* and direction D is calculated. If the constraints of (30) are satisfied, the diagnostic result will be figured out by D. For DSOC fault in the same phase, if the constraints of (31) are satisfied, the diagnostic result will be given according to the values of k_x, k_y, and k_{xy}. For DSOC faults in different phases, k_1 and k_2 are selected from abnormal slopes whose value is 1. The integrals of *origin-crossing*, k_1, k_2, and *Fault* represent durations of these signals, which are used for points identification and direction

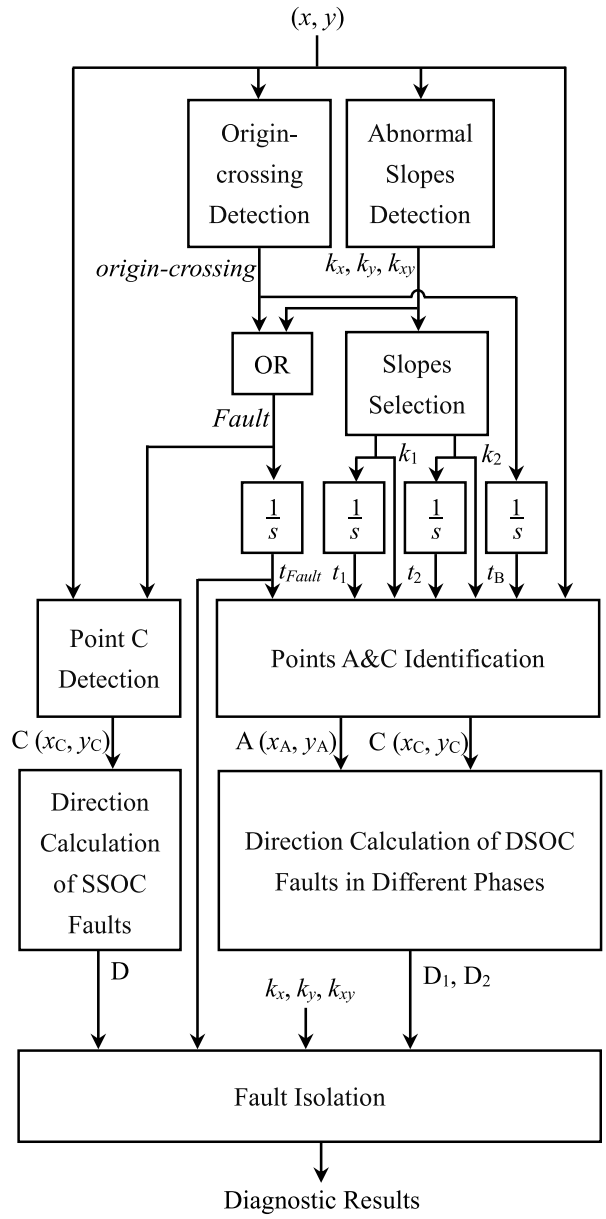

Fig. 4. Diagnosis process.

calculation. D_1 and D_2 are calculated after points A and C are identified. If the constraints of (32) are satisfied, the diagnostic result will be obtained by D_1 and D_2.

C. Load Variation Influence

Load variation has great impact on output currents, so as to change the size and even the shape of the trajectory. According to (14), the distance d from any point on the *a–b* trajectory to the origin increases linearly with the current I_{am}. If I_{am} increases, the trajectory expands. On the other hand, the trajectory shrinks. Within a short period of time after load changes, the transient process of output currents will lead to a distortion of the trajectory.

However, load variation has little influence on the diagnostic method. When load variation occurs under normal conditions,

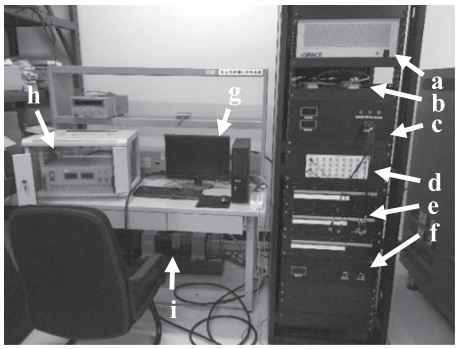

a. dSPACE b. Inverter c. Sensor box
d. DS2002 A/D Board e. DS4004 I/O Board
f. DC-side capacitor support
g. On-line faults diagnostic system
h. DC power i. Load

Fig. 5. General view of the experimental system.

the trajectory will gradually change to another size, but it will not pass through the origin; slopes of several consecutive points on it will not satisfy any of three slope anomaly conditions. Therefore, load variation will not lead to the false alarm under normal conditions.

When load variation occurs under fault conditions, there is at least one phase current that is close to zero. Although other phase currents will change, the points on the trajectory will only move on X axis, Y axis, or line $x + y = 0$; the direction calculations are not affected. In other words, load variation has no impact on fault detection and isolation.

From the beginning to the end of operations, some equipment on the train are in use and can never be interrupted, such as air conditioners, fans, etc. Therefore, the case of no load is hardly encountered unless the train completely stops working. In addition, even if air conditioners are shut down, there are still small no-load currents as long as the locomotive works. The method based on the calculation of abnormal slopes and directions is feasible as long as the output has current flow.

VI. Experimental Results

A. Experimental Set-Up

In order to verify the diagnostic method, an experimental system is set up based on dSPACE platform. The experimental system is shown in Fig. 5. The system consists of three parts: dSPACE, software, and hardware. dSPACE includes DS1007 processor board, DS2002 high precision A/D board, and DS4004 high speed I/O board. DS1007 is the core of dSPACE. This system communicates with the outside world through DS2002 and DS4004. Software part contains Simulink platform and the control desk. The control algorithm and the online diagnostic method based on the prototype are adapted into an online simulation model in dSPACE after they are approved in Simulink. The control desk can monitor the collected signals in real time and adjust the parameters. Hardware part is comprised of an adjustable dc power supply, an inverter, a dc-side capacitor support, a sensor box, and load. The key parameters of the prototype are shown in Table V.

TABLE V
Key Parameters of the Prototype

Parameters	Values
$T_1 - T_6$	MG100Q1JS40
Trigger IC	1ED020I12FA
Input voltage	600 VDC
Controller	$f_r = 50$ Hz
	$f_c = 3$ kHz
	Modulation index is 0.8
Load	Three-phase 380 VAC
	Active power is 15 kW
	Power factor is 0.85

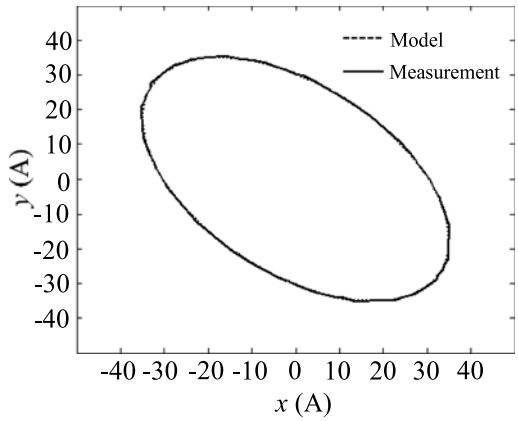

Fig. 6. Comparison between actual trajectory and calculated trajectory.

TABLE VI
Diagnosis of SSOC Faults

Fault	Point C (x_C , y_C)	Calculated direction	Diagnostic result
T_1	(–5.2, 32.3)	↑	FAULT_T1
T_2	(–34.5, 27.0)	↖	FAULT_T2
T_3	(–28.3, –4.1)	←	FAULT_T3
T_4	(5.0, –34.1)	↓	FAULT_T4
T_5	(33.2, –26.2)	↘	FAULT_T5
T_6	(27.9, 4.8)	→	FAULT_T6

In the experiment, SSOC faults are set by six fault simulation signals from the computer. DSOC faults are simulated by setting two SSOC faults at the same time. There are six kinds of SSOC faults and 15 kinds of DSOC faults in the experiment. Useless harmonics in the output currents are eliminated by digital low-pass filters. The variable α is set to $4\pi/9$ considering the requirements of output stability. The number of consecutive sampling points is set to 10. The following contents are verified:

1) Under normal operation, the *a–b* trajectory calculated by the mathematical model is basically the same as that recorded in the experiment.
2) All the *a–b* trajectories of SSOC faults and DSOC faults in Tables I and II are consistent with those in the experiment.

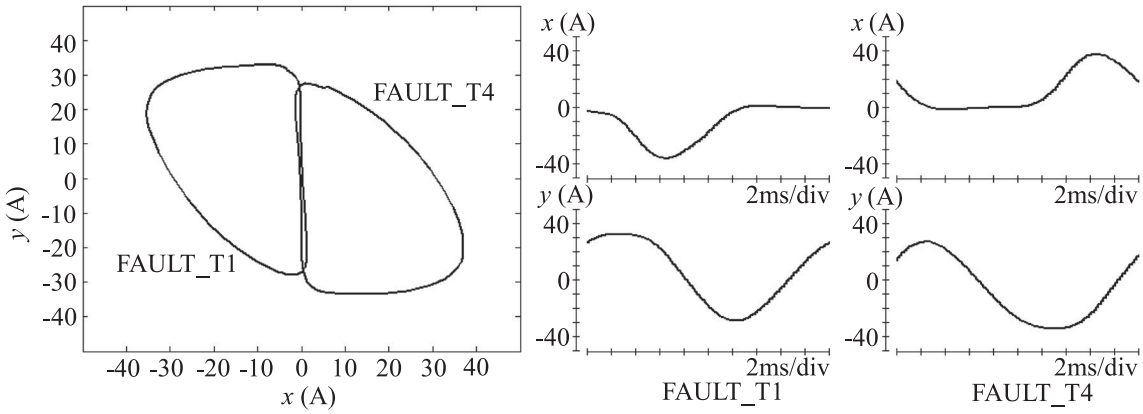

Fig. 7. *A–B* trajectories of FAULT_T1 and FAULT_T4.

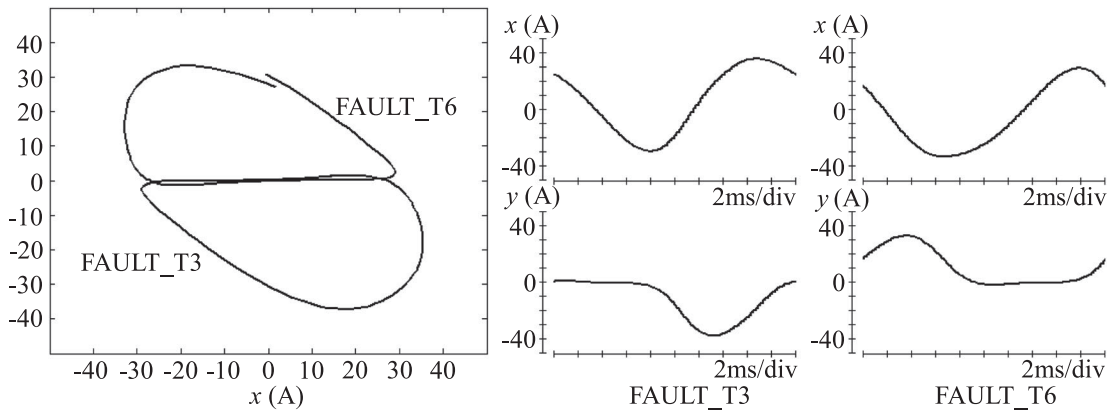

Fig. 8. *A–B* trajectories of FAULT_T3 and FAULT_T6.

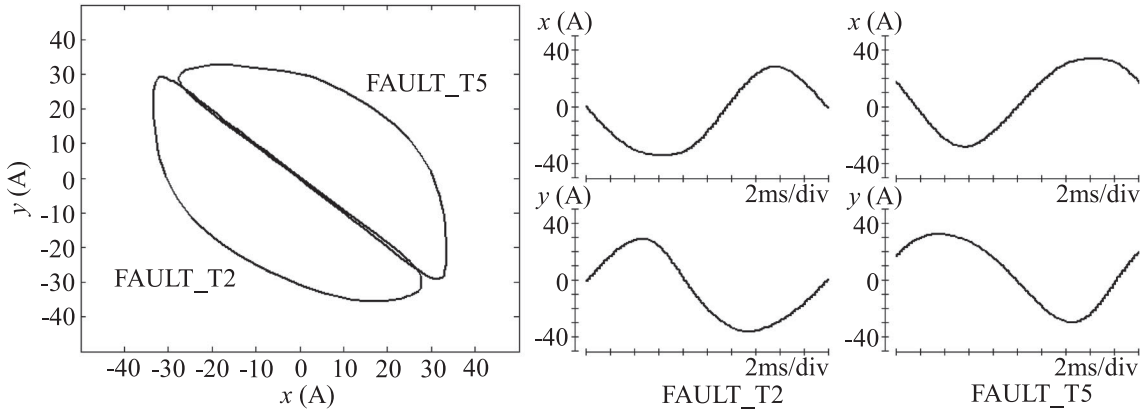

Fig. 9. *A–B* trajectories of FAULT_T2 and FAULT_T5.

TABLE VII
DIAGNOSIS OF DSOC FAULTS IN THE SAME PHASE

Fault	Fault time	Abnormal slopes	Diagnostic result
T_1 and T_4	$t_{Fault} > 0.01$ s	$k_x = 0, k_y = 1, k_{xy} = 0$	FAULT_T1&T4
T_3 and T_6	$t_{Fault} > 0.01$ s	$k_x = 1, k_y = 0, k_{xy} = 0$	FAULT_T3&T6
T_2 and T_5	$t_{Fault} > 0.01$ s	$k_x = 0, k_y = 0, k_{xy} = 1$	FAULT_T2&T5

All the faults can be diagnosed accurately by the method proposed in this paper.

3) Load variation has little impact on the diagnostic method.

B. Model Validation

Under normal operation, *a–b* trajectories are shown in Fig. 6. It can be seen that *a–b* trajectory calculated by the mathematical

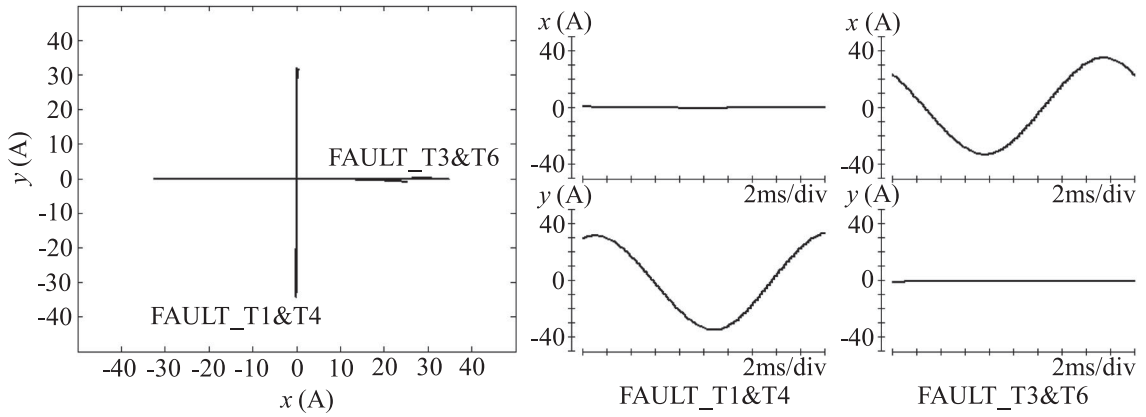

Fig. 10. *A–B* trajectories of FAULT_T1&T4 and FAULT_T3&T6.

model agrees with the recorded one. Through calculation, the angle θ (rad) of the actual trajectory is –0.707, and the centrifugal rate e is 0.817. Thus, the model proposed in this paper is accurate.

C. Diagnosis of SSOC Faults

Diagnostic results of all the SSOC faults are presented in Table VI. It lists the values of point C, the calculated directions according to these points, and the final diagnostic results. As we can see, point C of FAULT_T1 or FAULT_T4 is close to Y axis, the two directions are opposite, one points to the Y axis direction, the other points to the negative direction of Y axis. Point C of FAULT_T3 or FAULT_T6 is close to X axis, one direction points to the negative direction of X axis, the other points to the X axis. Point C of FAULT_T2 or FAULT_T5 is close to the line $x + y = 0$, the two directions are opposite as well. For each fault, the direction was accurately figured out and the fault was located successfully. All the *a–b* trajectories and their original signals in a certain period of time are shown in Figs. 7–9; they give a more visual diagnosis.

D. Diagnosis of DSOC Faults

Diagnostic results of DSOC faults in the same phase are presented in Table VII. It lists the fault time, values of abnormal slopes, and the diagnostic results. All t_{Fault} were detected more than half of the period; results were easily obtained after the values of abnormal slopes were calculated. The results show that all the diagnoses were accurate. Figs. 10 and 11 show *a–b* trajectories and their original signals of these faults in a certain period of time. These trajectories are consistent with those in Table II.

Diagnostic results of DSOC faults in different phases are presented in Table VIII. It lists the values of points A and C, the calculated directions, and the diagnosis results. It can be seen that the faults were located accurately according to these calculated directions. The *a–b* trajectories and original signals of these faults in a certain period of time are shown in Fig. 12–Fig. 16, and Fig. 17. These trajectories are also consistent with those in Table II.

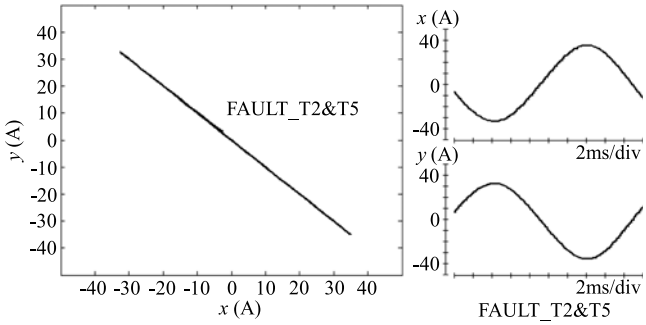

Fig. 11. *A–B* trajectories of FAULT_T2&T5.

E. Load Variation Influence

It has been proved that the proportion of *a–b* trajectory is affected by load variation, while the angle and the centrifugal rate are not. Three *a–b* trajectories were recorded under the condition of rated load, heavy load, and light load to verify the correctness of the theoretical analysis. These trajectories are shown in Fig. 18. The corresponding calculations of angle and centrifugal rate are listed in Table IX. It can be concluded that, under normal conditions, the size of the trajectory shrinks while the angle and the centrifugal rate remain constant.

There is a transient process in which the trajectory transfers from one steady state to another after load was changed. Fig. 19 shows two kinds of transient processes under normal conditions. Adjustable load of about 4 kW was added and cut off. During the process, the trajectory expanded or shrank gradually and slopes of several consecutive points on the trajectory were normal. There was no origin-crossing or abnormal slope signal detected. The transient process under normal conditions did not result in false alarm. Therefore, the method will not consider load variation as any OC fault under normal conditions.

The transient process under fault conditions will not affect the method as well. Fig. 20 shows the diagnosis process of T_1 OC fault. The fault was set at the red point and x gradually reduced to zero. Then, load was changed at the yellow point. It had certain impact on y but did not cause any obvious change to x when x was close to zero. After a period of time, the values of point C are

TABLE VIII
DIAGNOSIS OF DSOC FAULTS IN DIFFERENT PHASES

Faults	Point A (x_A , y_A)	Point C (x_C , y_C)	Calculated directions	Diagnostic result
T_1 and T_6	(–23.9, 1.4)	(–3.4, 30.4)	→↑	FAULT_T1&T6
T_3 and T_4	(22.6, –1.1)	(0.1, –26.0)	←↓	FAULT_T3&T4
T_1 and T_3	(1.5, –26.6)	(–15.8, –0.1)	↑←	FAULT_T1&T3
T_4 and T_6	(0.8, 18.8)	(14.5, –0.1)	↓→	FAULT_T4&T6
T_1 and T_5	(–26.4, 24.7)	(–0.1, 18.4)	↘↑	FAULT_T1&T5
T_2 and T_4	(28.9, –27.1)	(0.1, –18.6)	↖↓	FAULT_T2&T4
T_1 and T_2	(1.5, –23.1)	(–23.1, 22.8)	↑↖	FAULT_T1&T2
T_4 and T_5	(–1.4, 22.8)	(23.6, –22.0)	↓↘	FAULT_T4&T5
T_2 and T_6	(–24.7, –1.6)	(–16.5, 15.9)	→↖	FAULT_T2&T6
T_3 and T_5	(25.1, 1.8)	(14.6, –15.0)	←↘	FAULT_T3&T5
T_2 and T_3	(27.4, –25.9)	(–23.4, –0.2)	↖←	FAULT_T2&T3
T_5 and T_6	(–24.6, 23.6)	(25.4, 0.3)	↘→	FAULT_T5&T6

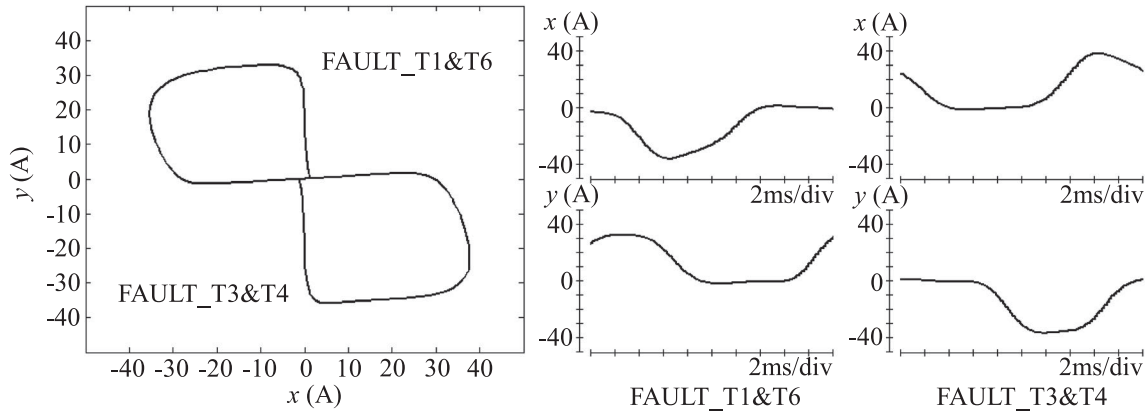

Fig. 12. *A*–*B* trajectories of FAULT_T1&T6 and FAULT_T3&T4.

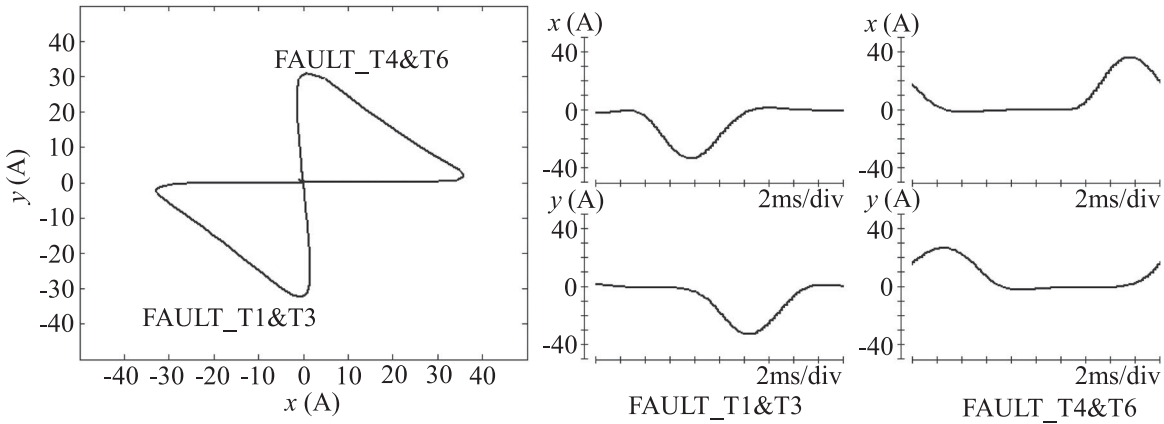

Fig. 13. *A*–*B* trajectories of FAULT_T1&T3 and FAULT_T4&T6.

detected and the fault was isolated as scheduled. As seen in the figure, the whole process from inverter failure to fault isolation took less than 0.01 s. Fig. 21 shows the diagnosis process of T_1 and T_4 OC faults. T_1 and T_4 were in the same phase. Faults were set at the red point and load was changed at the yellow point. Load variation did not affect x. After some time, faults were detected. When the fault time was detected more than 0.01 s, the current abnormal slopes were calculated according

TABLE IX
CALCULATION RESULTS OF ELLIPTIC ANGLE AND CENTRIFUGAL RATE UNDER THREE KINDS OF LOAD CONDITIONS

Load condition	Angle θ (rad)	Centrifugal rate e
Rated load	–0.707	0.817
Heavy load	–0.707	0.817
Light load	–0.707	0.817

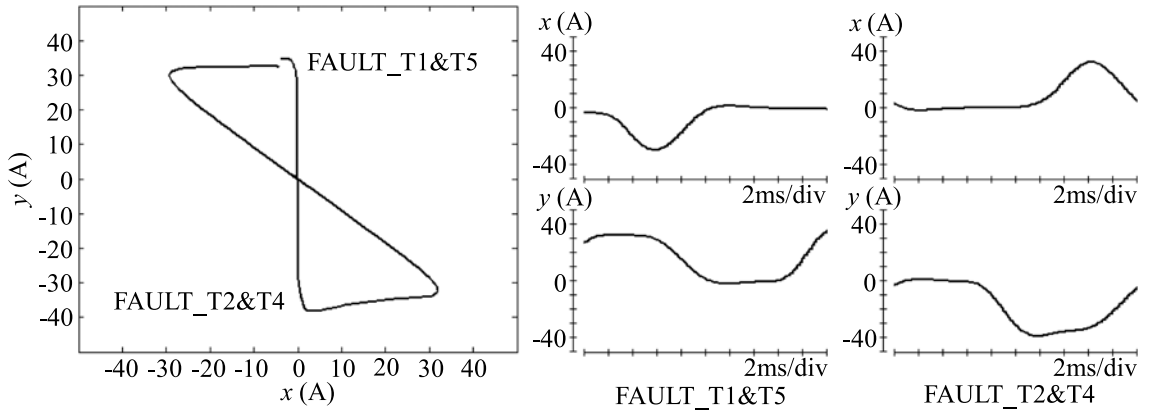

Fig. 14. *A–B* trajectories of FAULT_T1&T5 and FAULT_T2&T4.

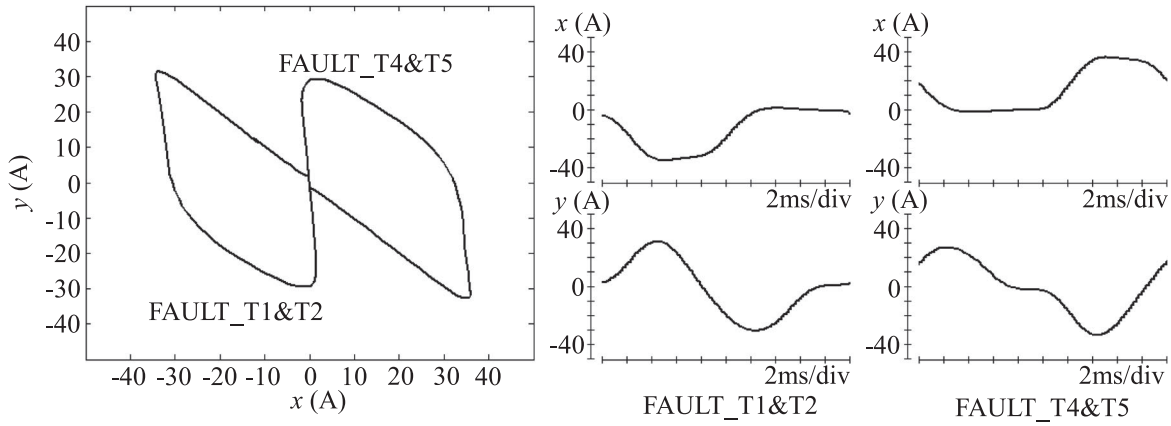

Fig. 15. *A–B* trajectories of FAULT_T1&T2 and FAULT_T4&T5.

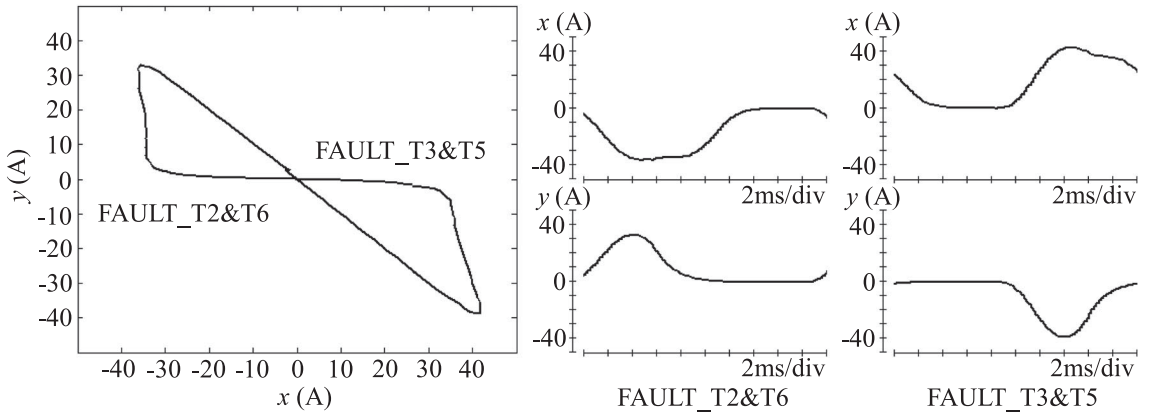

Fig. 16. *A–B* trajectories of FAULT_T2&T6 and FAULT_T3&T5.

to the values of x and y, then faults were isolated. The whole process took about 0.014 s. Fig. 22 shows the diagnosis process of T_1 and T_6 OC faults. T_1 and T_6 were in different phases. Load was changed at the yellow point after faults were set. P_1 was detected first at the blue point. After a period of time, P_2 was detected and faults were soon isolated at the green point. Load variation did not have any influence on the diagnostic results. The diagnostic process took less than 0.017 s. It can be seen from these results that the diagnostic method has certain robustness when load variation occurs.

VII. Conclusion

In this paper, an online diagnostic method is proposed based on *a–b* trajectories of inverter on a type 25T train. Under nor-

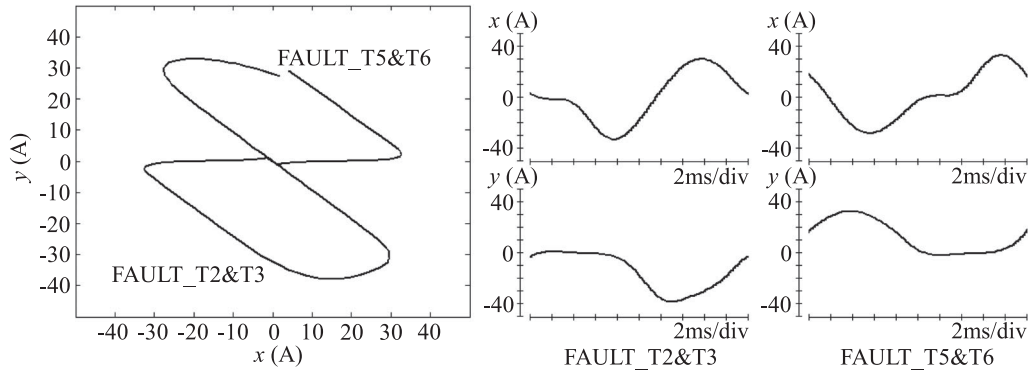

Fig. 17. *A–B* trajectories of FAULT_T2&T3 and FAULT_T5&T6.

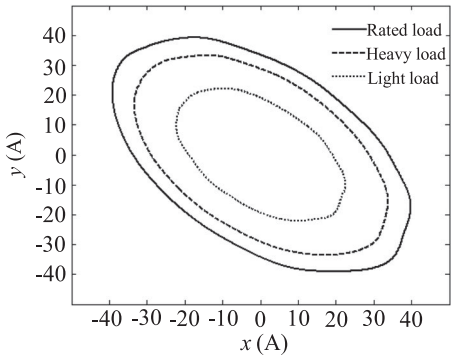

Fig. 18. *A–B* trajectories under three kinds of load conditions.

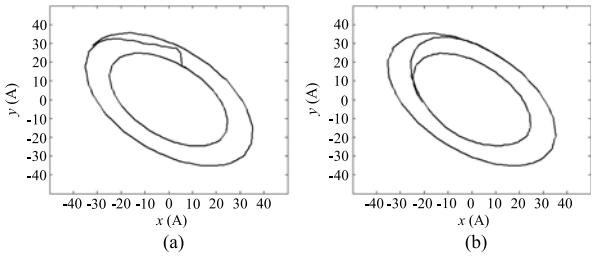

Fig. 19. Load variation impact on *a–b* trajectory under normal conditions. (a) Load was added. (b) Load was cut off.

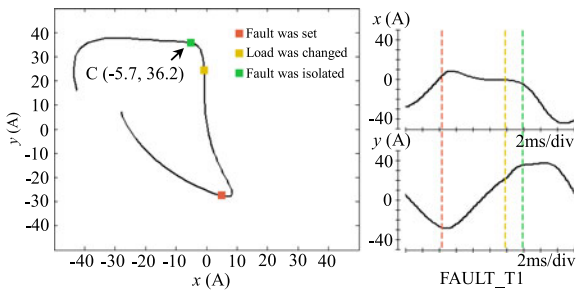

Fig. 20. Load variation impact on *a–b* trajectory when T_1 failed.

mal conditions, *a–b* trajectory is an ellipse centered at the origin in the Cartesian coordination. Its angle and centrifugal rate are fixed. All the *a–b* trajectories of both SSOC faults and DSOC faults are obtained by mathematical models. They are proved to be different from each other. Fault features irrelevant to load variation are extracted. Faults can be isolated successfully by

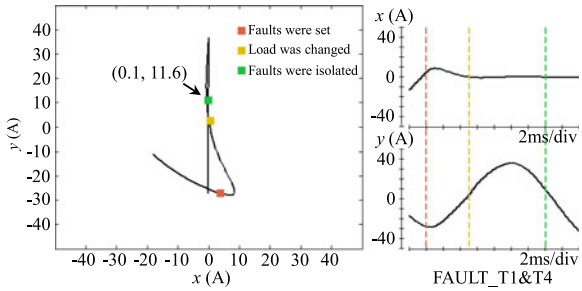

Fig. 21. Load variation impact on *a–b* trajectory when T_1 and T_4 failed.

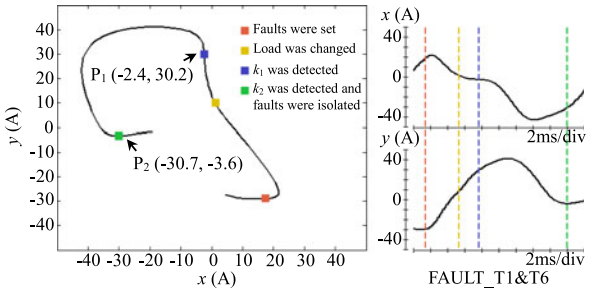

Fig. 22. Load variation impact on *a–b* trajectory when T_1 and T_6 failed.

identifying abnormal slopes and directions of these *a–b* trajectories. The fastest diagnostic process takes less than half a period. This method is robust to load change. In the experiments, the accuracy of the model and the effectiveness of the method are verified on dSPACE platform.

REFERENCES

[1] P. Wikstrom, L. A. Terens, and H. Kobi, "Reliability, availability, and maintainability of high-power variable-speed drive systems," *IEEE Trans. Ind. Appl.*, vol. 36, no. 1, pp. 231–241, Jan./Feb. 2000.

[2] Q. Q. Tang, S. C. Yan, and S. S. Lu, "Open-circuit fault diagnosis of transistor in three-level inverter," *Proc. CSEE*, vol. 28, no. 21, pp. 26–32, Jul. 2008.

[3] F. Abrahamsen, F. Blaabjerg, K. Ries, and H. Rasmussen, "Fuse protection of IGBT's against rupture," in *Proc. IEEE Nordic Workshop Power Ind. Electron.*, 2000, pp. 64–68.

[4] T. Kamel, Y. Biletskiy, and L. C. Chang, "Fault diagnoses for industrial grid-connected converters in the power distribution systems," *IEEE Trans. Ind. Electron.*, vol. 62, no. 10, pp. 6496–6507, Apr. 2015.

[5] T. Kamel, Y. Biletskiy, and L. C. Chang, "Fault diagnosis and on-line monitoring for grid-connected single-phase inverters," *Electr. Power Syst. Res.*, vol. 126, pp. 68–77, Sep. 2015.

[6] T. Kamel, Y. Biletskiy, and L. C. Chang, "Real-time diagnosis for open-circuited and unbalance faults in electronic converters connected to residential wind systems," *IEEE Trans. Ind. Electron.*, vol. 63, no. 3, pp. 1781–1792, Nov. 2016.
[7] L. Xiao and R. Li, "Research on the open-circuit fault diagnosis of transistor in inverter paralleling system," *Proc. CSEE*, vol. 26, no. 4, pp. 99–104, Feb. 2006.
[8] F. Zidani, D. Diallo, M. E. H. Benbouzid, and R. Nait-Said, "A fuzzy-based approach for the diagnosis of fault modes in a voltage-fed PWM inverter induction motor drive," *IEEE Trans. Ind. Electron.*, vol. 55, no. 2, pp. 586–593, Jan. 2008.
[9] W. Sleszynski, J. Nieznanski, and A. Cichowski, "Open-transistor fault diagnostics in voltage-source inverters by analyzing the load currents," *IEEE Trans. Ind. Electron.*, vol. 56, no. 11, pp. 4681–4688, Jun. 2009.
[10] J. O. Estima and A. J. M. Cardoso, "A new approach for real-time multiple open-circuit fault diagnosis in voltage-source inverters," *IEEE Trans. Ind. Appl.*, vol. 47, no. 6, pp. 2487–2494, Sep. 2011.
[11] D. R. Espinoza-Trejo, D. U. Campos-Delgado, E. Ba´rcenas, and F. J. Martinez-Lopez, "Robust fault diagnosis scheme for open-circuit faults in voltage source inverters feeding induction motors by using non-linear proportional-integral observers," *IET Power Electron.*, vol. 5, no. 7, pp. 1204–1216, Oct. 2012.
[12] S.-M. Jung, J.-S. Park, H.-W. Kim, K.-Y. Cho, and M.-J. Youn, "An MRAS-based diagnosis of open-circuit fault in PWM voltage-source inverters for PM synchronous motor drive systems," *IEEE Trans. Power Electron.*, vol. 28, no. 5, pp. 2514–2526, Aug. 2013.
[13] Q.-T. An, L. Sun, and L.-Z. Sun, "Current residual vector-based open-switch fault diagnosis of inverters in PMSM drive systems," *IEEE Trans. Power Electron.*, vol. 30, no. 5, pp. 2814–2827, Sep. 2015.
[14] F. Wu, J. Zhao, and Y. Liu, "Symmetry-analysis-based diagnosis method with correlation coefficients for open-circuit fault in inverter," *Electron. Lett.*, vol. 51, no. 21, pp. 1688–1690, Oct. 2015.
[15] H. T. Eickhoff, R. Seebacher, A. Muetze, and E. G. Strangas, "Enhanced and fast detection of open circuit faults in inverters for electric drives," in *Proc. 2016 IEEE Transp. Electrific. Conf. Expo*, Dearborn, MI, USA, 2016, pp. 1–6.
[16] C. G. Huang, F. Wu, J. Zhao, and D. H. Zhou, "A novel fault diagnosis method in SVPWM voltage-source inverters for vector controlled induction motor drives," *Int. J. Appl. Electromagn. Mech.*, vol. 50, no. 1, pp. 97–111, Jan. 2016.
[17] K. T. Hu, Z. G. Liu, and S. S. Lin, "Wavelet entropy-based traction inverter open switch fault diagnosis in high-speed railways," *Entropy*, vol. 18, no. 3, pp. 78–97, Mar. 2016.
[18] B. Gou *et al.*, "Load-current-based current sensor fault diagnosis and tolerant control scheme for traction inverters," *Electron. Lett.*, vol. 52, no. 20, pp. 1717–1719, Sep. 2016.
[19] R. Lúcio de Araujo Ribeiro, C. Brandão Jacobina, E. Roberto Cabral da Silva, and A. M. N. Lima, "Fault detection of open-switch damage in voltage-fed PWM motor drive systems," *IEEE Trans. Power Electron.*, vol. 18, no. 2, pp. 587–593, Mar. 2003.
[20] S. Karimi, P. Poure, and S. Saadate, "Fast power switch failure detection for fault tolerant voltage source inverters using FPGA," *IET Power Electron.*, vol. 2, no. 4, pp. 346–354, Jul. 2009.
[21] Q.-T. An, L.-Z. Sun, K. Zhao, and L. Sun, "Switching function model-based fast-diagnostic method of open-switch faults in inverters without sensors," *IEEE Trans. Power Electron.*, vol. 26, no. 1, pp. 119–126, Jun. 2010.
[22] J. Hang, J. Z. Zhang, M. Cheng, and S. Ding, "Detection and discrimination of open-phase fault in permanent magnet synchronous motor drive system," *IEEE Trans. Power Electron.*, vol. 31, no. 7, pp. 4697–4709, Sep. 2016.
[23] M. Abul Masrur, Z. Chen, and Y. Murphey, "Intelligent diagnosis of open and short circuit faults in electric drive inverters for real-time applications," *IET Power Electron.*, vol. 3, no. 2, pp. 279–291, Feb. 2010.
[24] B. B. Li, S. L. Shi, B. Wang, G. Wang, W. Wang, and D. Xu, "Fault diagnosis and tolerant control of single IGBT open-circuit failure in modular multilevel converters," *IEEE Trans. Power Electron.*, vol. 31, no. 4, pp. 3165–3176, Jul. 2016.
[25] M. Salehifar and M. Moreno-equilaz, "Fault diagnosis and fault-tolerant finite control set-model predictive control of a multiphase voltage-source inverter supplying BLDC motor," *ISA Trans.*, vol. 60, pp. 143–155, Nov. 2015.
[26] F. Wu and J. Zhao, "A real-time multiple open-circuit fault diagnosis method in voltage-source-inverter fed vector controlled drives," *IEEE Trans. Power Electron.*, vol. 31, no. 2, pp. 1425–1437, Apr. 2015.
[27] J. Zhang, J. Zhao, D. Zhou, and C. Huang, "High-performance fault diagnosis in PWM voltage-source inverters for vector-controlled induction motor drives," *IEEE Trans. Power Electron.*, vol. 29, no. 11, pp. 6087–6099, Jan. 2014.
[28] M. Trabelsi, M. Boussak, and M. Gossa, "PWM-switching pattern-based diagnosis scheme for single and multiple open-switch damages in VSI-fed induction motor drives," *ISA Trans.*, vol. 51, no. 2, pp. 333–344, Dec. 2011.

Xun Wu was born in Xinhua, China, on November 5, 1993. He received the B.E. degree in electrical engineering, in 2015, from the Central South University, Changsha, China, where he is currently working toward the Ph.D. degree in traffic information engineering and control in the Institute of Rail Transport and Electric Traction Technology.

His research interests include control techniques and fault diagnosis of power electronic converters, and life-prediction of capacitors.

Rui Tian was born in Fenyang, China, on March 27, 1992. She received the B.E. degree in electrical engineering, in 2015, from the Central South University, Changsha, China, where she is currently working toward the master's degree in electrical engineering in the Institute of Rail Transport and Electric Traction Technology.

Her research interests include fault diagnosis of power electronic converters and traction transformers.

Shu Cheng was born in Changsha, China, in 1981. He received the B.E. degree in automation form the East China University of Science and Technology, Shanghai, China, in 2003, and the M.S. and Ph.D. degrees in electrical engineering from the Central South University, Changsha, China, in 2006 and 2011, respectively.

He is currently an Associate Professor in the School of Traffic and Transportation Engineering, Central South University. His main research interests include fault diagnosis and fault-tolerant control of electrical drivers, and electric traction control technology.

Tefang Chen was born in Lianyuan, China, in 1957. He received the B.E. degree in automation form the Dalian University of Technology, Dalian, China, in 1981, and the M.S. and Ph.D. degrees in electrical engineering from the Central South University, Changsha, China, in 1991 and 2005, respectively.

Since 1982, he has been a Permanent Researcher in the Institute of Rail Transport and Electric Traction Technology, and is currently a Professor in the School of Traffic and Transportation Engineering, Central South University. His main research interests include fault diagnosis and fault-tolerant control of electrical drivers, and electric traction control technology.

Li Tong was born in Linfen, China, in 1957. He received the master's degree in power system and Automation from the Beijing Jiaotong University, Beijing, China, in 1997.

He is currently working as the Chief Engineer in the Locomotive and Vehicle Research Institute of China Railway Research Institute, Beijing, China, and the Deputy General Manager in the Beijing Zhongheng Electro-mechanical Technology Development Company, Beijing, China. His research interests include traction and network control system of EMU for high-speed train.